FDG-PET for Evaluating the Antitumor Effect of Intraarterial 3-Bromopyruvate Administration in a Rabbit VX2 Liver Tumor Model

Hee Sun Park, MD[1]
Jin Wook Chung, MD[1]
Hwan Jun Jae, MD[1]
Young Il Kim, MD[1]
Kyu Ri Son, MD[1]
Min Jong Lee, MD[1]
Jae Hyung Park, MD[1]
Won Jun Kang, MD[2]
Jung Hwan Yoon, MD, PhD[3]
Hesson Chung, PhD[4]
Kichang Lee, DVM, PhD[5]

Index terms:
Liver neoplasm, therapeutic radiology
Liver, interventional procedure
Liver, PET

Korean J Radiol 2007;8:216-224
Received July 4, 2006; accepted after revision August 1, 2006.

[1]Department of Radiology, Seoul National University College of Medicine, Institute of Radiation Medicine, Seoul National University Medical Research Center and Clinical Research Institute, Seoul National University Hospital, Seoul 110-744, Korea; [2]Department of Nuclear Medicine, Seoul National University College of Medicine, Seoul 110-744, Korea; [3]Department of Internal Medicine, Seoul National University College of Medicine, Seoul 110-744, Korea; [4]Biomedical Research Center, Korea Institute of Science and Technology, Seoul 139-774, Korea; [5]Department of Veterinary Radiology, Chonbuk National University College of Veterinary Medicine, Chonbuk 561-756, Korea

This study was supported by a grant of the National R&D Program for Cancer Control, Ministry of Health & Welfare, Republic of Korea.

Address reprint requests to:
Jin Wook Chung, MD, Department of Radiology, Seoul National University College of Medicine, 28, Yongon-dong, Chongno-gu, Seoul 110-744, Korea.
Tel. (822) 2072-2584
Fax. (822) 743-6385
e-mail: chungjw@radcom.snu.ac.kr

Objective: We wanted to investigate the feasibility of using FDG-PET for evaluating the antitumor effect of intraarterial administration of a hexokinase II inhibitor, 3-bromopyruvate (3-BrPA), in a rabbit VX2 liver tumor model.

Materials and Methods: VX2 carcinoma was grown in the livers of ten rabbits. Two weeks later, liver CT was performed to confirm appropriate tumor growth for the experiment. After tumor volume-matched grouping of the rabbits, transcatheter intraarterial administration of 3-BrPA was performed (1 mM and 5 mM in five animals each, respectively). FDG-PET scan was performed the day before, immediately after and a week after 3-BrPA administration. FDG uptake was semiquantified by measuring the standardized uptake value (SUV). A week after treatment, the experimental animals were sacrificed and the necrosis rates of the tumors were calculated based on the histopathology.

Results: The SUV of the VX2 tumors before treatment (3.87 $\pm$1.51 [mean $\pm$ SD]) was significantly higher than that of nontumorous liver parenchyma (1.72 $\pm$ 0.34) ($p < 0.0001$, Mann-Whitney *U* test). The SUV was significantly decreased immediately after 3-BrPA administration (2.05 $\pm$1.21) ($p = 0.002$, Wilcoxon signed rank test). On the one-week follow up PET scan, the FDG uptake remained significantly lower (SUV 1.41 $\pm$0.73) than that before treatment ($p = 0.002$), although three out of ten animals showed a slightly increasing tendency for the FDG uptake. The tumor necrosis rate ranged from 50.00% to 99.90% (85.48% $\pm$15.87). There was no significant correlation between the SUV or the SUV decrease rate and the tumor necrosis rate in that range.

Conclusion: Even though FDG-PET cannot exactly reflect the tumor necrosis rate, FDG-PET is a useful modality for the early assessment of the antitumor effect of intraarterial administration of 3-BrPA in VX2 liver tumor.

Hepatocellular carcinoma (HCC) is one of the most common, lethal malignancies throughout the world. The prognosis for patients with HCC is generally poor, with fewer than 10% of patients surviving five years after diagnosis, and the median survival period is 4–6 months for patients with unresectable tumors (1–3). Since very few of these patients (10–15%) are candidates for the surgery, transcatheter arterial chemoembolization (TACE) has been widely used for treating hepatic tumors, especially when the tumors are not surgically resectable (4, 5). However, the therapeutic efficacy of TACE in HCC is still limited and the overall results of treatment remain unsatisfactory (6). Therefore, a new strategy for the treatment of HCC is needed.

Highly malignant tumors exhibit the capacity to metabolize glucose to lactate at much higher rates than normal cells, and this high glucose metabolic rate is determined

by the hexokinase levels (7). Hexokinase catalyzes the first step in the glycolytic pathway by converting glucose to glucose 6-phosphate, which serves as fuel for the glycolytic pathway for the production of adeuosine triphosphate (ATP) and as a precursor for many biosynthetic processes that are essential for rapid tumor growth (8–10). Rapidly growing hepatomas are known to exhibit a high glucose catabolic rate (11). Type II hexokinase isoenzyme is a form of hexokinase that binds to the outer mitochondrial membrane, and it is predominantly overexpressed in hepatomas (12–15). Recent studies have demonstrated that 3-bromopyruvate (3-BrPA) inhibits tumor glycolysis by directly acting at the hexokinase level (16), and direct intraarterial delivery of 3-BrPA was shown to be a safe and effective strategy for treating VX2 tumor in a rabbit liver tumor model (17).

Positron emission tomography (PET) is a molecular imaging technique that provides images of physiologic processes. 18F-2-fluoro-2-deoxy-D-glucose (FDG) is a radiopharmaceutical analogue of glucose, and it is metabolized in a similar fashion to glucose in that FDG is transported across cell membranes by glucose transporter proteins and it is then phosphorylated (18). The rate of FDG uptake by the tumor cells is proportional to their metabolic activity. FDG is phosphorylated like glucose to form FDG-6-phosphate, but unlike glucose, it is not further metabolized and instead becomes trapped in metabolically active cells (19, 20). Because of the similarity of FDG to glucose, glucose metabolic rates can be quantified with PET imaging and so they can be applied for evaluating tumors with a high glucose catabolic rate.

There has been a recent report on the antitumor effect of 3-BrPA via intraarterial administration in rabbit VX2 liver tumor (17), but the analysis was done by pathology only and not with FDG-PET. Another report proved the feasibility of employing FDG-PET to evaluate the antitumor effect of 3-BrPA via intraperitoneal or direct infusion in rabbit AS-30D tumor (21). However, to the best of our knowledge, reports on the role of FDG-PET for evaluating the antitumor effect of intraarterial administration of 3-BrPA have not yet been published. Therefore, the purpose of our study was to investigate the feasibility of using FDG PET for evaluating the antitumor effect of a hexokinase II inhibitor, 3-BrPA, in experimentally induced liver tumor via intraarterial drug administration.

MATERIALS AND METHODS

VX2 Liver Tumor Model

The study was approved by the animal care committee of Seoul National University Hospital. The rationale for selecting VX2 liver tumor as the experimental model is as follows: its blood supply is similar to that of human hepatoma, it grows rapidly and becomes a sizable tumor that's easily identified by imaging, and it has a high glycolysis rate and elevated levels of mitochondrial bound hexokinase, which are characteristics of advanced stage tumors (8). In addition, catheter manipulation in a rabbit is relatively easy in the hepatic artery from the common femoral artery for delivering pharmacological agents (8, 11). Thirteen adult New Zealand white rabbits weighing 2.5–3.0 kg each were used. The VX2 carcinoma strain had been maintained by means of successive transplantation into the hind limbs of carrier rabbits. Anesthesia was induced with intravenous ketamine hydrochloride (50 mg per kilogram of body weight; Ketamine, Yuhan, Korea) and 2% xylazine (0.1 ml/kg; Rompun, Bayer, Germany). 0.1 ml of minced VX2 carcinoma was implanted through a midline subxyphoid incision into the subcapsular parenchyma of the left medial lobe of the liver. This method allows the growth of a single solitary, well-demarcated tumor in the liver of each recipient rabbit (11). The animals were used for experiments two weeks after the tumor implantation, when the tumors were expected to be a round shape 15–30 mm in diameter.

CT Evaluation of the Tumor Volume and the Enhancement Pattern

One day before intraarterial administration of 3-BrPA, spiral CT was performed (MX 8000; Philips Medical Systems, Best, The Netherlands) with the animals in the supine position. Nonenhanced CT was performed to cover the entire liver (3 mm collimation, 1.5 pitch and a 1 mm reconstruction interval). For contrast enhanced CT, 13 ml of contrast material (Iopromide, Ultravist; Schering, Berlin, Germany) was injected at a rate of 0.5 ml/sec through the auricular vein by an autoinjector (CT 9000 ADV Digital Injection System, Liebel-Flarsheim, Cincinnati, OH). With using a bolus tracking technique, a hepatic arterial and portal venous phase image was obtained at 16-second intervals.

On the CT scan, the location and the size of the tumor was measured by two radiologists working in consensus. The volume (V) of the tumor was calculated by the equation $V = L \times S^2/2$, where L and S are the the shortest and longest diameters, respectively, of the tumor (22). On the basis of calculated tumor volume, the animals were divided into two groups, i.e. the low dose and high dose 3-BrPA groups, to induce various degrees of tumor necrosis. Animals with similar sized tumors were evenly distributed to each group to minimize any possible bias. A total of ten rabbits were treated with intraarterial administration of 3-

BrPA, since three animals expired during the CT or PET scans or during the procedures: a low dose was 1 mM of 3-BrPA (n = 5), and a high dose was 5 mM of 3-BrPA (n = 5). The dose of 3-BrPA was determined according to the results of experiments performed by Ko et al., where complete inhibition of glycolytic activity of the VX2 tumor was induced with 5 mM of 3-BrPA (16). No control group was included in this experiment. Along with the volume measurements, the enhancement pattern of each tumor, as compared with the background liver, was also evaluated on the hepatic arterial and portal venous phases. Follow up CT scan was done one week later after 3-BrPA administration.

Intraarterial Administration of 3-BrPA

The concentrations of 3-BrPA (Aldrich Chemical Co., Cat. No. 238341) in the 1 mM and 5 mM administrations were prepared with sterile PBS (phosphate-buffered saline). The solution was sterilized with using a Sartorius' Minisart 0.2 um filter unit. Freshly made solutions were used in all of the studies.

Two weeks after the implantation of VX2 tumor in liver, fluoroscopy-guided intraarterial injection of 3-BrPA was performed at an angiography suite. Under the general anesthesia, surgical arteriotomy was done to expose the right common femoral artery, into which a 5-Fr dilator was placed as a substitute for an arterial sheath. Celiac arteriography was performed using a 2-Fr microcatheter (Progreat Microcatheter, Terumo, Japan), to identify the hepatic arterial anatomy and the feeding artery of the tumors. The left hepatic artery was selectively catheterized via the common hepatic artery. After the catheter was advanced to an appropriate position in the left hepatic artery, freshly made 3-BrPA solution (1 mM and 5 mM, 25 ml each) was infused directly into the targeted artery for two minutes. The catheter was then removed and the femoral artery was ligated. The animals were monitored after the procedure and they were given analgesics (intramuscular injections of 1–2 mg of meloxicam; Mobic®; Boehringer Ingelheim, Germany) when they showed signs of physical distress.

FDG-PET Protocol

FDG-PET scanning was done with a scanner (ECAT EXACT 47; Siemens CTI, Knoxville, TN) that had an intrinsic axial resolution of 6.2 mm and it could image 47 contiguous, 3.4-mm-thick planes simultaneously for a longitudinal field of view of 16.2 cm. All the rabbits fasted at least 24 hours prior to the study, and their bladders were emptied by insertion of 5 Fr Foley catheter. The entire procedure was done under general anesthesia. Before the administration of FDG, transmission scanning of the whole body was performed by using a 68Ge (Germanium-68) rod source for attenuation correction. Emission scans were obtained 45 minutes after the injection of 37 mBq of FDG. Image reconstruction was performed with an iterative reconstruction ordered-subset expectation maximization (OSEM)-based algorithm that included 16 subsets and six iterations. OSEM was performed with a Gaussian filter. Regions of interests (ROIs) were placed in the center of the tumor (crystal size: $4 \times 4 \times 20$ mm, pixel size: $2.57 \times 2.57 \times 3.37$ mm). PET images (transverse, coronal and sagittal) were reconstructed by using segmented attenuation correction and the images were corrected for decay. Scanning was performed three times for the experiment; the day before, immediately after and a week after the administration of 3-BrPA. PET scanning before and after treatment followed the CT scanning on the same day.

FDG-PET Data Analysis

Liver CT scans were used to localize the tumor before PET was performed. Two qualified physicians who were experienced in nuclear medicine and who were unaware of pathologic results, but they were aware of the CT findings, interpreted the PET scans. The images were reviewed in the transverse, coronal, and sagittal planes by using an interactive video display system (SPARC station 10; Sun Microsystems, Mountain View, CA). Interpretation included the semiquantification of the FDG uptake by using the peak standardized uptake value (SUV) on the emission images obtained 45 minutes after injection of FDG. After visually finding an area of the highest FDG uptake, the physician outlined a region of interest on the area of the highest uptake. An SUV normalized for the injected dose and body weight was obtained for each pixel by using a following method; SUV = ROI activity/(injected dose/body weight), where the ROI activity was measured in millicuries per milliliter, the injected dose was measured in millicuries and the body weight was measured in grams. The maximum pixel value of the ROI was chosen as the peak SUV. The SUV decrease rate of each tumor was obtained by using the following formula; the SUV decrease rate = (1-SUV of post-treatment/SUV of pre-treatment) $\times$ 100, and this was calculated immediately after and a week after treatment. The SUV of the initial treatment, the SUVs immediately after and at a week after treatment and SUV decrease rate immediately after and at a week after treatment were correlated with the tumor necrosis rate (Spearman rank correlation test).

Evaluation of the Antitumor Effect

Follow up CT was performed at one week after the

administration of 3-BrPA; the change of enhancement pattern on each phase was observed. The animals were sacrificed for histologic investigation with an overdose of pentobarbital sodium (Pentothal; Choong Wae Pharmacy, Seoul, Korea). Tumor volumes after the treatment were measured on the cut surface of the specimens and these were compared with those observed on CT before treatment. The antitumor effects were evaluated with using microscopic methods. The whole livers of the rabbits were explanted and fixed in 10% buffered formaldehyde solution. The part of the liver that contained the tumor was sliced at 5 mm-intervals in the axial plane that corresponded to the plane of the CT scan, and the sections were completely embedded in paraffin for histologic examination, after which the 4 μm-thick sections were stained with hematoxylin and eosin. Histologic changes and the extent of residual viable tumor was assessed via visual inspection by an experienced pathologist. To quantify the antitumor effects, the proportion of the viable tumor versus that of the entire tumor was estimated. The overall proportion of viable tumor was calculated on the basis of the average of the percentage in each slice. The tumor necrosis rate was defined as 100-viable tumor proportion (%).

Statistical Analysis

Differences between subgroups were examined by using the Mann Whitney *U* test and the Wilcoxon signed rank test. Univariate correlations were examined by using Spearman's rank correlation test. A p value of less than 0.05 was considered as a statistically significant difference. Statistical data analyses were performed with MedCalc for Windows (MedCalc Software, Mariakerke, Belgium).

RESULTS

CT Findings and Correlation with the Tumor Necrosis Rate

Chronological changes of the tumor volumes and enhancement pattern on CT, as well as the SUV in each animal, are described in Table 1. The CT observed volumes of the tumors before treatment ranged from 862.41 to 4,851.00 mm^3 (2,094.59 $\pm$1,305.50 [mean $\pm$ SD]) and those tumor volumes after treatment on the pathologic specimens ranged from 451.25 to 2,916.00 mm^3 (1,395.75 mm^3 $\pm$839.96), and the volume decrease rate ranged from 0 to 56.32% (31.57% $\pm$20.11). Comparison of the change of tumor volumes on CT was not possible because the boundary of each tumor on CT was masked with the peritumoral ischemic changes caused by the drug infusion (Fig. 1). The tumor volumes were significantly decreased after treatment in all animals (p = 0.008, Wilcoxon signed rank test), but the volume decrease rate showed no correlation with the tumor necrosis rate (Spearman r = $-$0.32, p = 0.37)

Before treatment, eight out of ten tumors showed peripheral or septum-like enhancement on the hepatic arterial phase and washout on the portal venous phase, which is characteristic of hypervascular tumors (Fig. 1). On the one week follow up CT scans, all of these enhanced portions on the arterial phase had decreased or disappeared.

Table 1. Chronological Changes of VX2 Liver Tumor after 3-BrPA Administration

No.	Group	Tumor Volume (mm^3)		CT Enhancement Pattern (HAP/PVP)		SUV			Tumor Necrosis Rate (%)
		Initial (on CT)	1 week (on specimen)	Initial	1 week	Initial	Immediate	1 week	
1	low dose 3-BrPA (1 mM)	4,851.00	2,268.00	high/low*	high/low	3.84	1.47 (61.72†)	2.10 (45.31)	80.00
2		2,745.50	1,575.00	high/low	low/low	4.69	1.42 (69.72)	2.70 (42.43)	80.00
3		1,143.45	1,009.79	low/low	low/low	6.50	5.07 (22.00)	1.51 (76.77)	50.00
4		862.41	451.25	high/low	low/low	3.00	1.35 (55.00)	0.50 (83.33)	85.00
5		1,436.50	907.50	low/low	low/low	2.49	1.40 (43.78)	1.00 (59.84)	70.00
6	high dose 3-BrPA (5 mM)	3,240.00	2,916.00	high/low	low/low	3.26	0.99 (69.63)	1.00 (69.33)	96.00
7		2,123.58	1,267.47	high/low	low/low	3.42	2.00 (41.52)	1.95 (42.98)	99.00
8		2,708.57	2,250.00	high/low	low/low	6.33	2.91 (54.03)	0.41 (93.52)	99.90
9		927.34	405.00	high/low	low/low	2.85	2.47 (13.33)	1.70 (40.35)	95.00
10		907.50	907.50	high/low	low/low	2.27	1.45 (36.12)	1.20 (47.14)	99.90

Nate. —HAP = hepatic arterial phase, PVP = portal venous phase, SUV = standardized uptake value, * high (or low) = when density of the tumor is higher (or lower) than that of background liver parenchyma. †Rates of SUV decrease after treatment are given in the parentheses of each column of SUV.

FDG-PET Findings

The SUV of the initial tumors in all rabbits ranged from 2.27 to 6.50 (3.87 ±1.51 [mean ±SD]), and those of the nontumorous liver parenchyma ranged from 1.34 to 2.61 (1.72 ±0.34). The FDG uptake of the VX2 tumor was significantly higher than that of the nontumorous liver parenchyma ($p < 0.0001$, Mann-Whitney U test).

The SUV was significantly decreased immediately after 3-BrPA administration (before treatment: 3.87 ±1.51 [mean ±SD], immediately after treatment: 2.05 ±1.21, $p = 0.002$, Wilcoxon signed rank test). On the one week follow up PET scan, the FDG uptake remained significantly lower than that before treatment (1.41 ±0.73, $p = 0.002$), and the SUV was persistently decreased in seven rabbits, but it showed a slightly increasing tendency in three rabbits (animals 1, 2 and 6) (Fig. 2). The decrease rate of SUV in each tumor after 3-BrPA administration ranged from 13.33 to 69.72 immediately after treatment and from 40.35 to 93.52 a week after treatment (Table 1).

Tumor Necrosis Rate

Under microscopic examination, the tumors after 3-

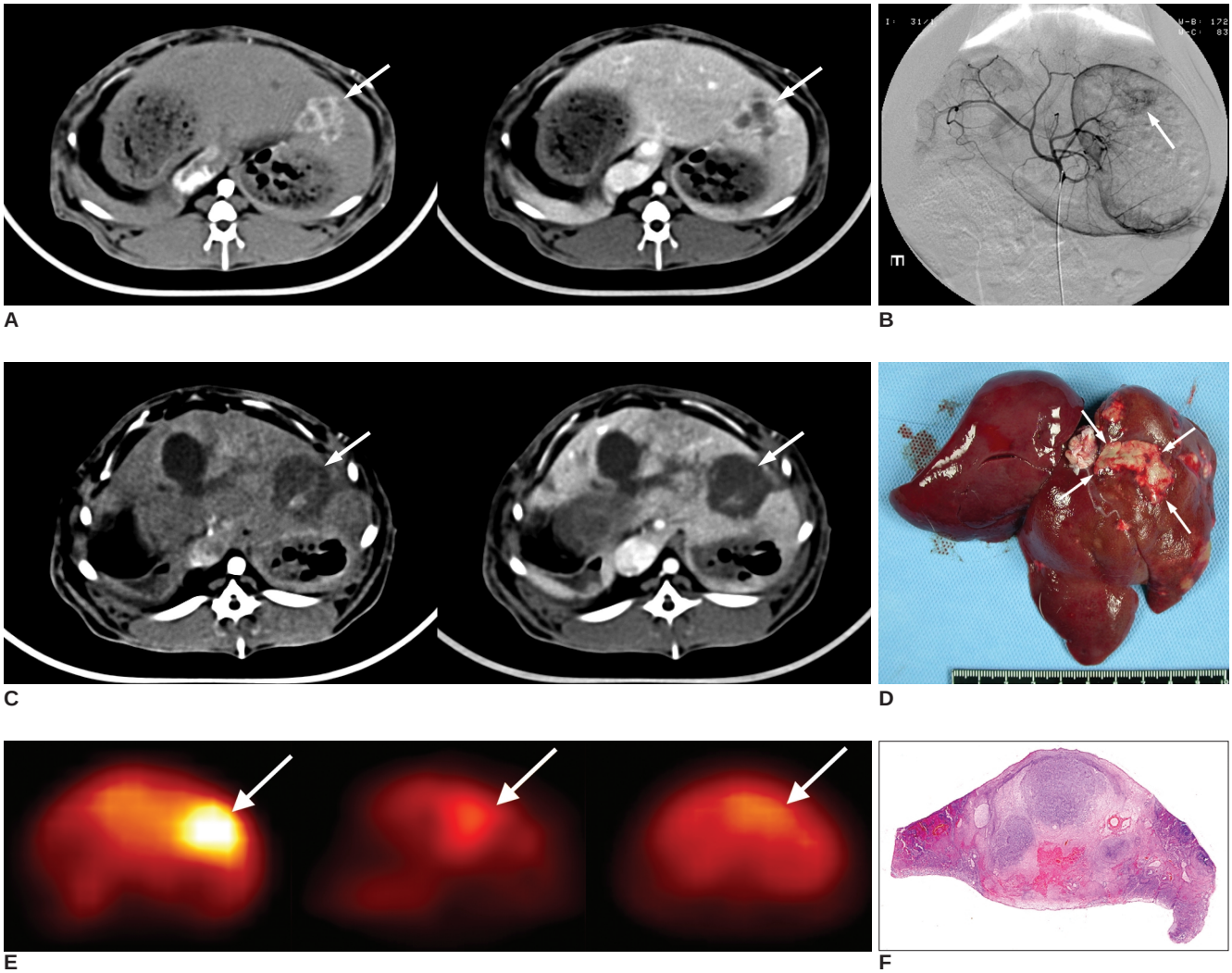

Fig. 1. A. Axial CT scan before treatment, the hepatic arterial phase (left) and the portal venous phase (right). Tumor is well demarcated in the left lobe of the liver. It shows irregular peripheral and septal enhancement and central low attenuation in the arterial phase (left, arrow). On the portal venous phase, arterial enhancement of the tumor washed out (right, arrow).
B. Celiac arteriography shows hypervascular tumor staining in the left lobe of the liver (arrow).
C. On the axial CT scan one week after treatment, the enhancing portion on the arterial and portal phases has almost decreased and larger area of low attenuation is seen as drug infusion defect (arrows).
D. Gross specimen of the extracted liver shows massive necrosis of the tumor (arrows).
E. Serial axial scans of FDG PET. Before treatment (left), the tumor is hypermetabolic with a SUV of 3.42 (arrow). It decreased to 2.00 immediately after treatment (middle, arrow), and it decreased more to 1.95 a week after the treatment (right, arrow).
F. Hematoxylin-eosin staining of the cut surface of the specimen (x 1) revealed near total necrosis with a small proportion of residual viable tumor. The tumor necrosis rate was 99.00%.

BrPA administrations showed a marked decrease in the number of viable tumor cells and there was also replacement by degenerated cells and persistent cell debris that involved both the peripheral and central regions of the tumors. Viable tumor cells were also observed in all specimens. The tumor necrosis rate ranged from 50.00% to 99.90% (85.48% ±15.87 [mean ±SD]). In addition, varying degrees of inflammatory changes were observed around the tumor.

Correlation between SUV and FDG PET and the Tumor Necrosis Rate

The SUVs measured before, immediately after and a week after 3-BrPA administration did not show any statistically significant correlation (Spearman $r = 0.07$, $p = 0.83$, Spearman $r = 0.41$, $p = 0.22$, Spearman $r = -0.14$, $p = 0.69$, respectively). Likewise, the decrease rates of SUV immediately and one week after treatment and the tumor necrosis rate showed no significant correlation (Spearman $r = -0.29$, $p = 0.41$, Spearman $r = 0.49$, $p = 0.89$, respectively) (Fig. 3).

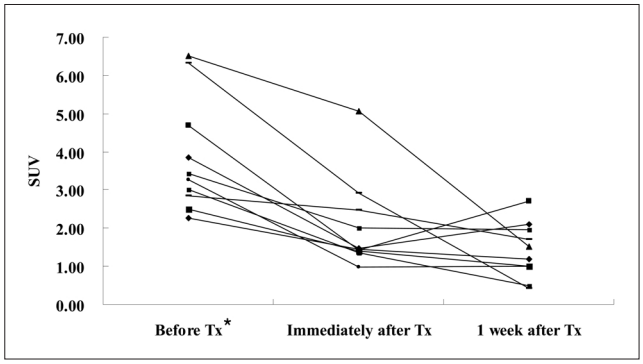

Fig. 2. Line graph shows the chronological SUV changes of the VX2 liver tumors in each animal. Seven animals showed a gradually decreased SUV, but the other three animals showed rising tendency of FDG uptake at one week after treatment. * Tx = treatment.

DISCUSSION

Antitumor Effect of 3-BrPA

The antitumor effect of 3-BrPA has already been demonstrated by in vitro and in vivo experiments. A study by Ko et al. revealed that 3-BrPA abolished cell ATP production by suppressing both glycolysis and oxidative phosphorylation via the inhibition of hexokinase II, and 3-BrPA facilitated cell death in in-vitro experiments using rat AS-30D cells and rabbit VX2 carcinoma cells (16). As for the mechanism of cell death, Gwak et al. have shown that 3-BrPA induced apoptosis of HCC cell lines through the activation of the mitochondrial apoptotic signaling cascades (23).

VX2 tumor, although it is of a non-hepatic origin, exhibits glucose metabolic properties that are characteristics of many rapidly growing hepatomas, of which the biochemical hallmarks are a high glycolytic/high hexokinase phenotype (13, 16). Geschwind et al. reported that direct intraarterial delivery of 3-BrPA to rabbit VX2 liver tumors selectively inhibited the viability of cells, without any significant damage to the surrounding liver tissue (17). In another recent study by Ko et al., the highly glycolytic HCC line of AS-30D tumor, which was grown either internally (in the abdominal cavity) or externally (in the upper back) in rats, was nearly completely eradicated by intraperitoneal or direct intratumoral injection of 3-BrPA (21).

The present study using VX2 carcinoma also demonstrated a marked antitumor effect by intraarterial injection of 3-BrPA. However, complete necrosis of the tumor was not achieved in any tumor by a single intraarte-

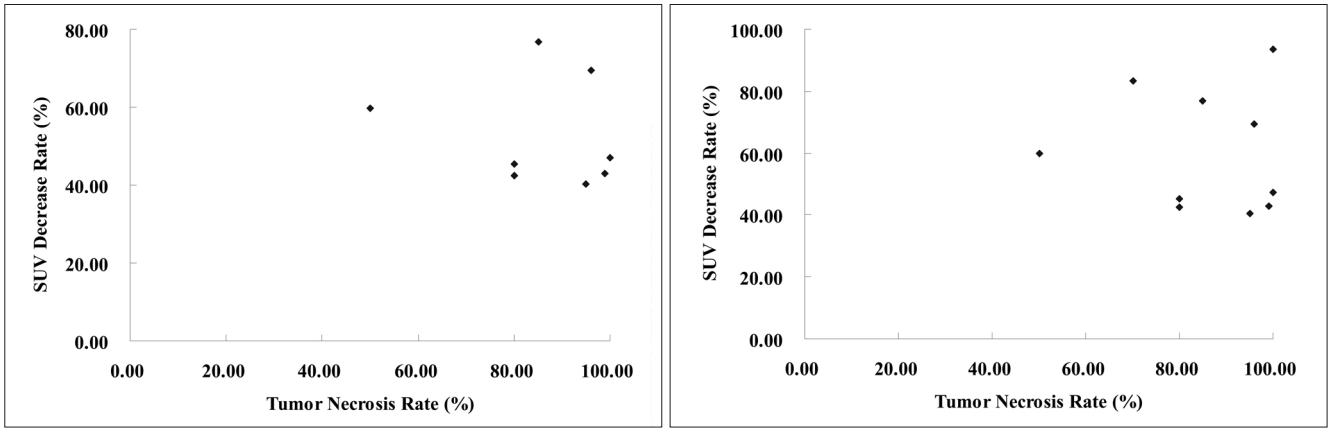

Fig. 3. Scatterplots show correlation between SUV and the tumor necrosis rate (%) immediately (**A**) and one week (**B**) after treatment. No significant correlation between these parameters was observed (Spearman $r = -0.29$, $p = 0.41$ in **A**, Spearman $r = 0.49$, $p = 0.89$ in **B**).

rial injection of 3-BrPA. In addition, the result of our study differed from that of Geschwind et al.'s study (17), in which nearly 100% tumor necrosis was obtained with delivery of 25 ml of 0.5 mM 3-BrPA; that study had similar tumor volumes and a shorter follow up period compared with those of our study, whereas the same proportion of tumor necrosis was achieved only when using ten times the dose of 3-BrPA in our study. This discrepancy between the studies remains to be solved with additional experiments.

Evaluation of the Antitumor Effect of 3-BrPA with CT and PET Imaging and the Pathologic Correlation

On this study, CT demonstrated limitations for evaluating the tumor response to intraarterial 3-BrPA administration. Comparison of the tumor volumes was not feasible because the peritumoral morphologic changes on CT made exact demarcation of the initial tumor difficult (Fig. 1). Even though we measured the post-treatment tumor volumes on each gross specimen and found that the tumor volume decreased after treatment, measurement errors caused by different modality could be unavoidable. The changes of the enhancement pattern on CT reflected the antitumor effect of 3-BrPA by showing a decrease or disappearance of arterial enhancement of the tumors (Table 1). However, considering those tumors that showed no residual enhancing part on post-treatment CT also had varying degrees of viable tumor on pathology, CT enhancement is not a reliable finding to monitor tumor response to 3-BrPA.

FDG was proven to be a suitable tumor-seeking agent in both experimental and human studies (24, 25). Since FDG accumulates in tumor tissue with increased glucose metabolism, it can provide a useful indication of tumor viability (26, 27). Oya et al. in their study reported that fluorine-18-FDG uptake by the VX2 liver tumors was 3.5 $\pm$0.9 times higher than that by the normal liver tissue; therefore, the tumor-nontumor contrast was good on PET scans (26).

There are important issues in PET imaging for an antitumor treatment of hypermetabolic liver tumors, that is, whether it is possible to predict its therapeutic effect in the early stage of the treatment and whether it can depict small residual viable tumor after treatment. Recent studies have demonstrated the value of FDG-PET for assessment of glucose metabolism in liver tumors and also the effects of treatment such as transcatheter arterial chemoembolization. Nagata et al. studied FDG-PET in patients with malignant liver tumor, and they reported that FDG-PET was more useful than other imaging methods and tumor markers as a functional imaging modality for monitoring. tumors (28). Okazumi et al. reported that the calculated rate constants of FDG in patients' liver tumors reflected the differentiation of HCC and this may be useful in quantitatively assessing tumor viability after treatment (29). Torizuka et al. compared FDG-PET and histological examination of HCC 3−45 days after TAE, and they suggested that those tumors with decreased or absent FDG uptakes were highly necrotic, and the PET findings reflected tumor viability more accurately than the extent of intratumoral iodized oil retention on CT images (30). Oya et al. reported that a marked decrease of FDG uptake corresponded with a decreased number of tumor cells after TAE and irradiation in VX2 liver tumor (31). In addition, Ko et al. in their recent study that was mentioned above, evaluated the antitumor effect of 3-BrPA with FDG-PET imaging in four rats with AS-30D tumors in their abdominal cavity and upper back via intraperitoneal or direct intratumoral administration (21). However, to the best of our knowledge, evaluation of the antitumor effect of intraarterial administration of 3-BrPA with FDG-PET imaging has not yet been reported on.

In this study, the FDG uptakes of all tumors before the treatment were significantly higher than those of the nontumorous liver parenchyma, indicating that VX2 liver tumor has a highly glycolytic activity, and this agreed with the data from previous reports on FDG-PET in VX2 tumor (24, 29).

SUV was significantly decreased immediately after 3-BrPA administration in all animals except one (animal 4), which implies that the therapeutic effect of intraarterial administration of 3-BrPA can be evaluated and semiquantified immediately after the procedure by means of FDG-PET imaging. In the one animal that did not show a significant immediate response to 3-BrPA administration (animal 4, SUV: 6.50 to 5.07), it was difficult to explain the delayed response on the one week follow up study.

On the one week follow up study, seven animals showed further decreases in FDG uptake, but the other three animals (animals 1, 2 and 6) showed a slight increase in FDG uptake compared with that of immediate post-treatment. On microscopic examination of the specimens, all of the treated animals had residual viable tumors, including the seven animals with persistent decrease in FDG uptake on the one-week follow up PET scans. These results indicate that immediate suppression of glycolysis by intraarterial administration of 3-BrPA does not necessarily mean ultimate tumor death after treatment and a single intraarterial injection of 3-BrPA induces only partial tumor necrosis of the tumor with interval re-growth of the residual viable tumor. Considering the incomplete tumor response after treatment, the intraarterial delivery of 3-

BrPA might not achieve the tumorocidal dose evenly in the entire tumor or it doesn't sustain the tumorocidal dose for enough time to induce complete tumor necrosis.

Another possible explanation for the increasing tendency of SUV in three animals in this study is the FDG uptake by peritumoral inflammatory cells. According to Spaepen et al., FDG uptake, as measured by SUV, correlated with the number of metabolically viable cells regardless of whether they were tumoral or non-tumoral in nature (32), and FDG uptake can also occur by the macrophages within a tumor mass, and especially after chemotherapy. Our histologic slide review revealed peritumoral inflammatory cell infiltrations in all animals. However, the degree of inflammation was not apparently higher in those three animals compared with the others, and it was not possible to differentiate the FDG uptake by the inflammatory cells from the viable tumor cells with the resolutions of the images in our study.

Against our expectation, we failed to demonstrate quantitative correlation between SUV or a decreased rate of SUV and the tumor necrosis rate after treatment. This may be due to inherent limitation of a FDG-PET scan to detect a small viable fraction of small tumors, or the SUV uptake by peritumoral inflammatory cells can be one of the reasons. In this study, the VX2 tumors showed a high tumor necrosis rate (mean: 85.48%) after intraarterial injection of 3-BrPA. According to the comparative study by Torizuka et al. of FDG-PET and the histological finding of HCC after TAE, an SUV ratio more than 0.6 suggested residual viable tumor, whereas an SUV ratio of 0.6 or less indicated more than 90% tumor necrosis (30). One thing to be noticed is that they covered tumors with a wide range of necrosis rates, from less than 25% to near 100%; when only the tumors with a higher necrosis rate (> 80%) were taken into consideration, quantitative correlation between FDG uptake and the tumor necrosis rate was not achieved either.

Limitations

There are potential limitations of this study that must be mentioned. First, the follow up period after 3-BrPA administration was too short since all the experimental animals were sacrificed together a week after the treatment for the histological correlation. Therefore, the FDG uptake after treatment was not correlated with other parameters when evaluating the therapeutic response, such as the tumor volume change and survival of the animals. Especially in case of the animals with an increasing tendency of FDG uptake a week after treatment, a longer period of follow up seems to be necessary for determining how the FDG uptake changes thereafter. Second, even though we used dual-phase liver CT for localizing tumors on PET scan, there were difficulties in accurately measuring the tumor areas and some errors happened when calculating the FDG uptake in tumors and the SUV. Moreover, since we used a conventional PET scanner in this animal study, errors due to partial volume artifacts were inevitable. A PET-CT scanner and an animal PET scanner with higher resolution may help reduce such errors.

CONCLUSION

Intraarterial administration of 3-BrPA in a VX2 liver tumor model showed an antitumor effect via suppression of glycolysis, and FDG-PET can be a useful modality for the early evaluation of this treatment, even though FDG-PET cannot exactly reflect the tumor necrosis rate.

References

1. Di Bisceglie AM, Rustgi VK, Hoofnagle JH, Dusheiko GM, Lotze MT. NIH conference. Hepatocellular carcinoma. *Ann Intern Med* 1988;108:390-401
2. Rustgi VK. Epidemiology of hepatocellular carcinoma. *Gastroenterol Clin North Am* 1987;16:545-551
3. Okuda K, Ohtsuki T, Obata H, Tomimatsu M, Okazaki N, Hasegawa H, et al. Natural history of hepatocellular carcinoma and prognosis in relation to treatment. Study of 850 patients. *Cancer* 1985;56:918-928
4. Ramsey DE, Kernagis LY, Soulen MC, Geschwind JF. Chemoembolization of hepatocellular carcinoma. *J Vasc Interv Radiol* 2002;13:S211-S221
5. Yamada R, Sato M, Kawabata M, Nakatsuka H, Nakamura K, Takashima S. Hepatic artery embolization in 120 patients with unresectable hepatoma. *Radiology* 1983;148:397-401
6. Bruix J. Treatment of hepatocellular carcinoma. *Hepatology* 1997;25:259-262
7. Pedersen PL. Tumor mitochondria and the bioenergetics of cancer cells. *Prog Exp Tumor Res* 1978;22:190-274
8. Arora KK, Pedersen PL. Functional significance of mitochondrial bound hexokinase in tumor cell metabolism. Evidence for preferential phosphorylation of glucose by intramitochondrially generated ATP. *J Biol Chem* 1988;263:17422-17428
9. Greiner EF, Guppy M, Brand K. Glucose is essential for proliferation and the glycolytic enzyme induction that provokes a transition to glycolytic energy production. *J Biol Chem* 1994;269:31484-31490
10. Mathupala SP, Rempel A, Pedersen PL. Glucose catabolism in cancer cells: identification and characterization of a marked activation response of the type II hexokinase gene to hypoxic conditions. *J Biol Chem* 2001;276:43407-43412
11. Weinhouse S. Glycolysis, respiration, and anomalous gene expression in experimental hepatomas: G.H.A. Clowes memorial lecture. *Cancer Res* 1972;32:2007-2016
12. Pedersen PL, Mathupala S, Rempel A, Geschwind JF, Ko YH. Mitochondrial bound type II hexokinase: a key player in the growth and survival of many cancers and an ideal prospect for therapeutic intervention. *Biochim Biophys Acta* 2002;1555:14-

20
13 Shinohara Y, Ichihara J, Terada H. Remarkably enhanced expression of the type II hexokinase in rat hepatoma cell line AH130. *FEBS Lett* 1991;291:55-57
14. Mathupala SP, Rempel A, Pedersen PL. Glucose catabolism in cancer cells. Isolation, sequence, and activity of the promoter for type II hexokinase. *J Biol Chem* 1995;270:16918-16925
15. Nakashima RA, Paggi MG, Scott LJ, Pedersen PL. Purification and characterization of a bindable form of mitochondrial bound hexokinase from the highly glycolytic AS-30D rat hepatoma cell line. *Cancer Res* 1988;48:913-919
16. Ko YH, Pedersen PL, Geschwind JF. Glucose catabolism in the rabbit VX2 tumor model for liver cancer: characterization and targeting hexokinase. *Cancer Lett* 2001;173:83-91
17. Geschwind JF, Ko YH, Torbenson MS, Magee C, Pedersen PL. Novel therapy for liver cancer: direct intraarterial injection of a potent inhibitor of ATP production. *Cancer Res* 2002;62:3909-3913
18. Gallagher BM, Fowler JS, Gutterson NI, MacGregor RR, Wan CN, Wolf AP. Metabolic trapping as a principle of oradiopharmaceutical design: some factors resposible for the biodistribution of [18F] 2-deoxy-2-fluoro-D-glucose. *J Nucl Med* 1978;19:1154-1161
19. Kapoor V, McCook BM, Torok FS. An introduction to PET-CT imaging. *Radiographics* 2004;24:523-543
20. Rohren EM, Turkington TG, Coleman RE. Clinical applications of PET in oncology. *Radiology* 2004;231:305-332
21. Ko YH, Smith BL, Wang Y, Pomper MG, Rini DA, Torbenson MS, et al. Advanced cancers: eradication in all cases using 3-bromopyruvate therapy to deplete ATP. *Biochem Biophys Res Commun* 2004;324:269-275
22. Okada M, Kudo S, Miyazaki O, Saino T, Ekimoto H, Iguchi H, et al. Antitumoral efficacy and pharmacokinetic properties of pirarubicin upon hepatic intra-arterial injection in the rabbit V x 2 tumour model. *Br J Cancer* 1995;71:518-524
23. Gwak GY, Yoon JH, Kim KM, Lee HS, Chung JW, Gores GJ. Hypoxia stimulates proliferation of human hepatoma cells through the induction of hexokinase II expression. *J Hepatol* 2005;42:358-364
24. Som P, Atkins HL, Bandoypadhyay D, Fowler JS, MacGregor RR, Matsui K, et al. A fluorinated glucose analog, 2-fluoro-2-deoxy-D-glucose (F-18): nontoxic tracer for rapid tumor detection. *J Nucl Med* 1980;21:670-675
25. Strauss LG, Conti PS. The applications of PET in clinical oncology. *J Nucl Med* 1991;32:623-648
26. Oya N, Nagata Y, Ishigaki T, Abe M, Tamaki N, Magata Y, et al. Evaluation of experimental liver tumors using fluorine-18-2-fluoro-2-deoxy-D-glucose PET. *J Nucl Med* 1993;34:2124-2129
27. Messa C, Choi Y, Hoh CK, Jacobs EL, Glaspy JA, Rege S, et al. Quantification of glucose utilization in liver metastases: parametric imaging of FDG uptake with PET. *J Comput Assist Tomogr* 1992;16:684-689
28. Nagata Y, Yamamoto K, Hiraoka M, Abe M, Takahashi M, Akuta K, et al. Monitoring liver tumor therapy with [18F]FDG positron emission tomography. *J Comput Assist Tomogr* 1990;14:370-374
29. Okazumi S, Isono K, Enomoto K, Kikuchi T, Ozaki M, Yamamoto H, et al. Evaluation of liver tumors using fluorine-18-fluorodeoxyglucose PET: characterization of tumor and assessment of effect of treatment. *J Nucl Med* 1992;33:333-339
30. Torizuka T, Tamaki N, Inokuma T, Magata Y, Yonekura Y, Tanaka A, et al. Value of fluorine-18-FDG-PET to monitor hepatocellular carcinoma after interventional therapy. *J Nucl Med* 1994;35:1965-1969
31. Oya N, Nagata Y, Tamaki N, Takagi T, Murata R, Magata Y, et al. FDG-PET evaluation of therapeutic effects on VX2 liver tumor. *J Nucl Med* 1996;37:296-302
32. Spaepen K, Stroobants S, Dupont P, Bormans G, Balzarini J, Verhoef G, et al. [(18)F]FDG PET monitoring of tumour response to chemotherapy: does [(18)F]FDG uptake correlate with the viable tumour cell fraction? *Eur J Nucl Med Mol Imaging* 2003;30:682-688